ENVIRONMENTAL RESEARCH
LETTERS

LETTER

# Contradictory influences of urbanization on intense convective rainfall in a subtropical city

**Qi Zhuang**[1,2,4,*], **Marika Koukoula**[2,*], **Shuguang Liu**[1], **Zhengzheng Zhou**[1], **Lisha Gao**[3] and **Nadav Peleg**[2,4]

[1] Department of Hydraulic Engineering, Tongji Univerisity, Shanghai, People's Republic of China
[2] Institute of Earth Surface Dynamics, University of Lausanne, Lausanne, Switzerland
[3] Shanghai Water Planning and Design Research Institute, Shanghai, People's Republic of China
[4] Expertise Center for Climate Extremes, University of Lausanne, Lausanne, Switzerland
[*] Authors to whom any correspondence should be addressed.

**E-mail:** qi.zhuang@unil.ch and marika.koukoula@unil.ch

**Keywords:** urbanization scenarios, convective rainfall intensification, Shanghai, WRF, extreme precipitation, urban heat island

Supplementary material for this article is available online

OPEN ACCESS

RECEIVED
17 May 2024

REVISED
9 August 2024

ACCEPTED FOR PUBLICATION
22 August 2024

PUBLISHED
30 August 2024



## Abstract

In light of the rapid growth in cities, there is a pressing need to explore how urbanization affects extreme weather, especially short-duration convective storms that can potentially trigger urban floods. Here we use a high-resolution Weather Research and Forecasting convection-permitting model to simulate 23 summer convective storms over the subtropical city of Shanghai, China. We simulated these events in three different scenarios: present urban, no-urban, and urban-expansion settings. Results show contradictory findings of urbanization's influence on convective rainfall, which is associated with urban-surroundings hydrothermal differences and diurnal cycles. Urban expansion further intensifies daytime convective rainfall when inhomogeneous temperature and moisture conditions between the city and its surroundings are present, whereas other conditions may suppress rainfall intensity. The findings provide the potential mechanisms of rainfall modification by urban expansion in subtropical cities, offering useful insights for urban planning and flood management in Shanghai and other rapidly urbanizing cities.

## 1. Introduction

More than half of the global population, 57% as of 2022, reside in urban areas, and this percentage is projected to increase to 68% by 2050 (United Nations 2018). Urban expansion has emerged as a highly significant driver of local climate (Fischer *et al* 2021, Liu *et al* 2022), leading to considerable changes in extreme rainfall (Zhang *et al* 2018, Georgescu *et al* 2021, Doan *et al* 2022) and rendering cities particularly vulnerable to flooding (IPCC, Intergovernmental Panel on Climate Change 2023). Hence, it is important to better understand how urbanization affects the local climate to aid future urban development in mitigating weather-related hazards.

The impacts of urban areas on rainfall and its mechanisms (both dynamic and thermodynamic) have been extensively examined via observational and modeling research (Qian *et al* 2022), beginning from the pioneering Metropolitan Meteorological Experiment led by Changnon *et al* (1971). However, both positive and negative impacts have been found. Many have observed an increase in rainfall due to the urban heat island effect (UHI, Oke 1982), i.e. when the temperature contrast between urban and rural areas results in a greater convergence of moisture into cities and enhances convection (Shem and Shepherd 2009, Shepherd *et al* 2010, Yang *et al* 2017). Other mechanisms that support rainfall intensification were also identified. For example, Niyogi *et al* (2011) and Yang *et al* (2019) showed that urban-induced surface roughness facilitates convergence and enhances rainfall over cities. Furthermore, aerosol concentrations that operate as cloud condensation nuclei have been found to enhance the amount of rainfall that falls in urban areas (Van den Heever and Cotton 2007). A meta-analysis of 85 quantitative studies revealed that rainfall intensification could occur over, downwind,

and/or upwind cities and that there is a variation across studies about the extent and specific location of the intensification (Liu and Niyogi 2019). This is supported by Shen and Yang (2023) in which four paradigms were developed to explain preferential locations of rainfall enhancement according to the dominance of urban-induced thermal perturbations and mechanical turbulence.

Conversely, several studies indicate a weakening impact of urban areas on rainfall, which is explained by moisture depression in the urban lower atmosphere (Guo *et al* 2006, Hand and Shepherd 2009, Georgescu *et al* 2012, Wang *et al* 2018), known as the urban dry island effect (i.e. UDI, Tapper 1990, Meili *et al* 2022, Hao *et al* 2023). Moreover, Wang *et al* (2012) and Zhang *et al* (2009) showed that an elevated atmospheric boundary layer over cities may result in enhanced homogeneity of water vapor in the lower troposphere, thus reducing the convective available potential energy and suppressing rainfall. Others indicated that rainfall could be suppressed due to urban air pollution, as high-concentration of aerosols can slow down the process of cloud-drop coalescence and the conversion of cloud water into rainfall (Givati and Rosenfeld 2004, Rosenfeld *et al* 2008).

The interaction between meteorological elements and the urban environment generates unique atmospheric conditions in local areas, making it challenging to identify specific components that regulate urban modifications to rainfall. For example, the UHI intensity in humid climate areas is more noticeable in comparison with other climates (Zhao *et al* 2014), potentially enhancing atmospheric instability and local convection. In coastal or lakefront cities, local circulations (i.e. sea/lake breezes) play a significant role in increasing the temperature gradient and complicating the local UHI effect (Shepherd and Burian 2003, Joseph *et al* 2008, Li *et al* 2013). Symmetric and asymmetric urbanization patterns could also affect the distribution of UHI intensity (Li *et al* 2016), and city shape coupled with inland/coastal environments led to different conclusions (Zhang *et al* 2022). Moreover, rainfall types (Li *et al* 2021), terrain characteristics (Freitag *et al* 2018), and pre-storm meteorological conditions (Shen and Yang 2023) could also jointly contribute to different urban impacts on rainfall magnitude and location.

The urban influence on rainfall is likely to be correlated with the size of the urban areas (Wang *et al* 2015, Han *et al* 2022). It is reasonable to hypothesize that cities observing rainfall enhancement should experience a greater degree of intensification with urbanization and urban expansion, though likely non-linear. However, this has not yet been confirmed because both contradicting UHI and moisture depression effects were found to increase with urban growth (Schmid and Niyogi 2013). For example in Beijing, Miao *et al* (2011) found that rainfall-enhancing effects are dominant when the city expands to a certain size, while Wang *et al* (2015) reached the opposite conclusion. Mixed impacts on rainfall as a result of urban growth have also been found in Houston, United States (Buran and Shepherd 2005), and in the Yangtze River Region, China (Han *et al* 2022). Our ability to generalize the impact of cities under different climates and rainfall types is far from comprehensive (Lalonde *et al* 2023).

In light of the gaps discussed above, we here explore how urban expansion is affecting rainfall intensities in Shanghai, a mega-city located in a subtropical climate. The frequency and amount of heavy rainfall in Shanghai have increased significantly due to urbanization (Liang and Ding 2017, Xu *et al* 2024). However, there is limited knowledge of the mechanism driving these rainfall changes and the potential effects of future urbanization on extreme rainfall. Using a convection-permitting model, we investigate how summer convective rainfall is affected in the city of Shanghai in the context of enhanced urbanization. We discuss the urbanization impacts on rainfall amounts and the underlying thermodynamic mechanisms.

## 2. Data and methodology

### 2.1. Study area

The study area extends around the mega-city of Shanghai located in the center of the Yangtze River Delta, China. It is the most populous city in China and has experienced dramatic urban and economic development over the past decades (Zhu *et al* 2016, Statista Search Department 2024, Zhu and Ling 2024). It has a typical subtropical climate, with a distinct rainfall season from May to September, influenced by subtropical monsoons, cyclonic storms, and heavy convective rainfall (Zhuang *et al* 2022). The eastern side of Shanghai resides next to the East China Sea, while a large shallow lake (i.e. Taihu Lake) is situated to the west. The intricate interaction between the water bodies and land results in a complex local circulation in this area (Zhong *et al* 2017, Zhao *et al* 2020, He *et al* 2022), making it challenging to comprehend the effects of Shanghai and its urbanization on the local rainfall.

### 2.2. Model set up

We use the Weather Research and Forecasting model (WRF, version 4.5, Skamarock *et al* 2019) coupled with a multi-layer urban canopy model (UCM) building effect parameterization (BEP, Martilli *et al* 2002). Initial and lateral boundary conditions for the model simulations are derived from the 6 h National Centers for Global Forecast System NCEP (2000, 2015), GFS, product, with 1° and 0.25° resolution in 2008–2014 and 2015–2022 respectively. The MODIS land cover product at 15 s spatial resolution (Broxton *et al* 2014)

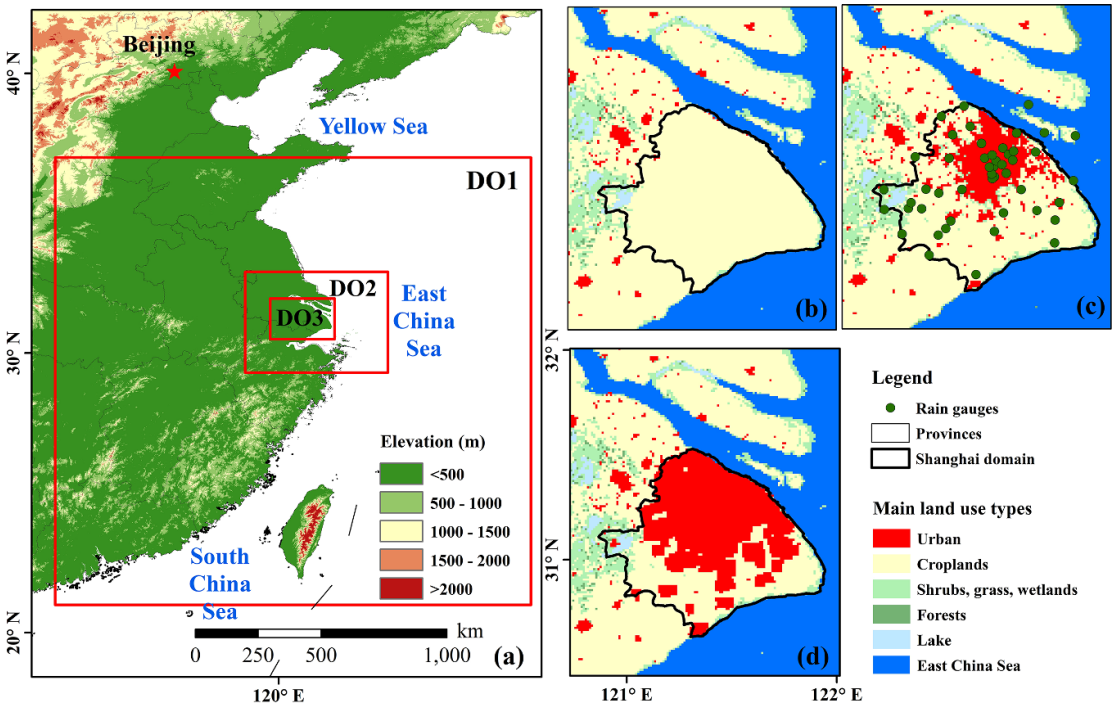


**Figure 1.** (a) Map of the study area and the three WRF simulation domains (DO1, DO2, and DO3). Main Land use and land cover within the analyzed domain for the (b) No-urban, (c) CTR, and (d) Urban-2 km scenarios.

**Table 1.** Model configurations and parameterization schemes.

| Physics | Scheme |
|---|---|
| Microphysics | Thompson scheme (Hong *et al* 2004) |
| Radiation | RRTMG (Mlawer *et al* 1997) |
| Cumulus parameterization | Kain–Fritsch (new Eta) scheme only for D01 (Kain 2004) |
| Land surface scheme | Noah-MP (Niu *et al* 2011) |
| Urban canopy model | Multilayer urban canopy scheme (BEP) (Martilli *et al* 2002) |
| Planetary boundary layer scheme | Yonsei University scheme (YSU) scheme (Hong *et al* 2004) |
| Surface layer physics | Revised MM5 Monin–Obukhov scheme (Chen and Dudhia 2001) |
| Nesting options | 3 nested domains (9 km, 3 km and 1 km) with one-way nesting |
| Surface lake physics | LAKE (Gu *et al* 2015) |
| Number of vertical layers | 45 |
| Spin up time | 18 h |

is used to define the land-use and land-cover. The WRF model is configured with 3 one-way nested domains (figure 1(a)): DO1 with a spatial resolution of 9 km (194 × 185 grids), DO2–3 km (136 × 166), and DO3—1 km (163 × 226). DO1 covers southeastern China, while DO3 covers Shanghai city and the surrounding Taihu Lake. The update frequency of boundary conditions of the three domains is 6 h. Vertically, the domains stretch up to 50 hPa with 45 layers. The physics options used in the simulations are summarized in table 1. Multiple scheme combinations were examined (see figure S1 in the supplementary material), but we presented only the setup that showed the highest agreement with the observations. The first 18 h of spin-up time are not considered in the analysis.

We first simulate rainfall events with the present land-use and urban area ('CTR' scenario, figure 1(c)). Then we set two other land-use scenarios to explore the impacts of urban expansion: a 'No-urban' scenario in which the urban area is replaced with croplands (figure 1(b)) and a 2 km urban expansion scenario, where grids within 2 km outside the city boundary are replaced with urban land cover grids ('Urban-2 km' scenario, figure 1(d)). The urban land use in Urban-2 km scenario is plausible and consistent with

the projected urban area data published by Chen *et al* (2020), under different Shared Socioeconomic Pathways that consider possible challenges associated with adaptation to climate change and its mitigation. It is consistent with the projected city area in 2050 under SSP1 (i.e. low urban development in the future), or in 2030 under SSP5 (i.e. highly developed scenario).

### 2.3. Rainfall and thermodynamic analyses

We simulate 23 heavy convective rainfall events that occurred during the summer months between 2008 and 2023. All the selected storms advected from west to east, often with a minor southeast wind component, representing the typical trajectories of summer convective storms in this region (Shen *et al* 2019, Li *et al* 2021b) (detailed in table S1). An illustrative example of several hourly time steps simulated at the finer (i.e. 1 km and 1 h) space-time resolution (domain in figure 1(c)) for the three urban scenarios is presented in figure S2. We focus on short-duration events, with a mean duration of around 7 h; 52% of the events last less than or equal to 6 h, and only one of the events lasts longer than 12 h. The spatial maximum accumulated rainfall of 23 storms varies from 25.8 mm to 339.5 mm, and all events move eastward. Hourly data from 47 ground gauges (figure 1(c)) provide the basis for the evaluation of the simulations. Using a point-to-point approach (i.e. comparing the accumulated rainfall from a rain gauge to the WRF grid where the rain gauge is positioned), we evaluate the overall performance of the CTR-simulated events (figure S3). The mean absolute error is quite high (20.4 mm; equivalent to 54% bias), largely due to a small number of simulated events that overestimate rainfall accumulations (as seen in figure S3 (c)). However, the CTR simulations are generally in agreement with observations and replicate convective rainfall dynamic processes (figure S3 (b)).

The impact of urban expansion on rainfall is assessed through the analysis of changes in rainfall accumulation $P$ [mm] over the urban domain $u$ (i.e. the area enclosed by the solid black line in figures 1(b)–(d)). The land and sea areas outside of the urban domain are referred to as the city's surroundings $s$ (see figure S4 for a breakdown of the urban and surrounding grid cells). The accumulated rainfall over the $u$ urban grid cell $i$ is defined as:

$$\hat{P}_i^u = \sum_{t=1}^{D} P_i^u(t), \tag{1}$$

where $P_i^u(t)$ is the simulated rainfall at time step $t$ at the $u$ urban grid cell $i$, and $D$ is the total number of time steps.

Moreover, we examine the differences between the No-urban and CTR scenarios (defined as $\Delta P_{u1}$), as well as between the CTR and Urban-2 km scenarios ($\Delta P_{u2}$), to analyze the response of the city expansion. To simplify the comparison, we examine the mean change in rainfall between scenarios, in the following way:

$$\delta P_{u1} = 100 \cdot \left( \frac{\sum_{i=1}^{n} \hat{P}_i^{u,\mathrm{CTR}}}{n} - \frac{\sum_{i=1}^{n} \hat{P}_i^{u,U0}}{n} \right) \Bigg/ \frac{\sum_{i=1}^{n} \hat{P}_i^{u,\mathrm{CTR}}}{n}, \tag{2}$$

and,

$$\delta P_{u2} = 100 \cdot \left( \frac{\sum_{i=1}^{n} \hat{P}_i^{u,U2\mathrm{km}}}{n} - \frac{\sum_{i=1}^{n} \hat{P}_i^{u,\mathrm{CTR}}}{n} \right) \Bigg/ \frac{\sum_{i=1}^{n} \hat{P}_i^{u,\mathrm{CTR}}}{n}, \tag{3}$$

where $n$ is the number of urban grid cells, and CTR, $U0$, and $U2$km refer to the control, No-urban, and Urban-2 km scenarios respectively.

The thermodynamic conditions that might explain the rainfall differences between scenarios are also examined. More specifically, the hourly low-level (i.e. 6 lowest vertical layers within 540 m above ground) temperature $T$ [°C] and water vapor mixing ratio $Q$ [kg kg$^{-1}$] are computed for the grid cells in both the urban domain and its surrounding areas:

$$\hat{T}_i^u(t) = \frac{\sum_{z=1}^{6} T_i^u(t,z)}{6}, \tag{4}$$

where $T_i^u(t,z)$ is the temperature $T$ at the $z$ vertical layer and hourly time step $t$ located at the $u$ urban grid cell $i$. $Q_i^u(t,z)$ is computed similarly; for the urban surroundings, the variables are computed the same way, except that the notation $u$ is replaced by $s$.

Additionally, we consider the omega $\omega$ [Pa s$^{-1}$] as an indication of convection. To that end, we average only the negative $\omega$ values for the 20 lowest vertical layers (i.e. up to 7.3 km above ground) in each grid cell:

$$\hat{\omega}_i^u(t) = \frac{\sum_{z=1}^{20} \omega_i^u(t,z)}{N}, \tag{5}$$

where $N$ is the number of layers with negative $\omega$. Positive $\omega$ values were excluded, as only negative values indicate upward vertical motion. We multiply equation (5) by $-1$, so greater positive $\hat{\omega}_i^u(t)$ values will express greater upward vertical motion (and vice versa). To examine differences in convection between the scenarios, we use $\Delta\omega_{u1}$, $\Delta\omega_{u2}$, by replacing the notation $P$ with $\omega$ in equations (2) and (3).

High inhomogeneity of thermodynamic conditions between urban areas and their surroundings may also lead to increased atmospheric instability and enhanced local convection. Consequently, we examine the level of variability in $T$ and $Q$ of all urban and surrounding grids shown in figure S5 for the CTR

scenario. To that end, we pool together all urban and surrounding values of $\hat{T}_i^u(t)$ and $\hat{T}_i^s(t)$ (according to equation (4)) for each rainfall event and computed the mean, 5th, and 95th percentiles (i.e. $T_\mu$, $T_5$, $T_{95}$ per event). We then average these values for all rainfall events falling into a given category (i.e. Increased-P and Decreased-P categories will be mentioned later), resulting in $\overline{T_\mu}$, $\overline{T_5}$, and $\overline{T_{95}}$ for each category. The differences $\overline{T_{95}} - \overline{T_\mu}$ and $\overline{T_\mu} - \overline{T_5}$ are finally computed and considered as a proxy of the inhomogeneity level of $T$ distributions contrast between the urban area and its surroundings during the storms. The same procedure is followed for $Q$.

Last, we examine the timing and causes of the rainfall and heat anomalies resulting from continued urban sprawling. We compute the diurnal disparity between the urban area and its surroundings for the temperature difference ($\Delta T_{u2}$) and rainfall anomalies only in the urban area ($\delta P_{u2}$) from the urban expansion scenarios following the same method mentioned above (equation (3)) but for each hour of the day.

## 3. Results

We begin by examining each storm individually to determine the effect of urbanization and the expansion of urban areas on rainfall by plotting box plots that summarize rainfall variability within the urban domain (figure S5). Considering the mean values of $\overline{\hat{P}_i^u}$ in each box plot, we have found that among the 23 storms, (i) Approximately 35% exhibit a monotonically increasing $\overline{\hat{P}_i^u}$ with urbanization—meaning that rainfall accumulation increases from No-urban to CTR scenarios and continues to increase from CTR to Urban-2 km scenarios (termed as 'Increased-P', shown as blue area in figure 2(a)); (ii) about 30% have the consistent decrease with urbanization, (i.e. 'Decreased-P'; red area in figure 2(a)); and (iii) about 35% of storms show a mixed response to urbanization—with half showing a rise in rainfall from No-urban to CTR followed by a decrease from CTR to Urban-2 km scenarios, while the other half showing the opposite trend ('Mixed-P'; gray area in figure 2(a)).

We then investigate whether changes in rainfall convection are in agreement with the urbanization-induced rainfall patterns described above by summarizing the change of $\omega$ values in urban grids under different scenarios. We found that the variation of $\overline{\hat{P}_i^u}$ with urbanization is consistent with the change in $\overline{\hat{\omega}_i^u(t)}$ (figure 2(b)). Comparing figures 2(a) and (b), the points with a positive (negative) $\overline{\hat{P}_i^u}$ and $\overline{\hat{\omega}_i^u(t)}$ are mostly located in the same quadrant. A positive correlation between rainfall enhancement and convection condition is found in the Increased-P group: on average, $\overline{\delta P_{u1}}$ (change from No-urban to CTR) increase by 17% and $\overline{\delta P_{u2}}$ (from CTR to Urban-2 km) increase by 12% with corresponding increases of 14% and 6% in $\overline{\delta\omega_{u1}}$ and $\overline{\delta\omega_{u2}}$. In the Decreased-P group, the decrease in $\overline{\delta P_{u1}}$ and $\overline{\delta P_{u2}}$ (by −19% and −15%, respectively) with urbanization being also associated with decline in $\overline{\delta\omega_{u1}}$ and $\overline{\delta\omega_{u2}}$ but the magnitude mismatched (−7% and −12%). Further details of the box plots for all $\hat{P}_i^u$ and $\hat{\omega}_i^u(t)$ in each group can be found in figure S5.

Next, we investigate the thermodynamic conditions associated with enhancing and suppressing convection and rainfall. In figure 2(c), the inhomogeneity level of $T$ and $Q$ for the CTR scenario are summarized in a radar plot, using $T_\mu$, $T_5$, and $T_{95}$ (and the equivalent $Q$ values, consistent with the mean, 5th, and 95th percentiles, respectively, as shown in each box plot in figure S6) as proxies for the two groups. For the Urban-2 km scenario, the variability is similar (not shown). As can be seen, events in the Increased-P group exhibit a higher level of inhomogeneity in both $T$ and $Q$ compared to those in the Decreased-P group (i.e. the blue area occupies a larger portion than the red area in figure 2(c)). Specifically, $\overline{T_{95}} - \overline{T_5}$ is equal to 5.5 °C in the Increased-P, which is 2.1 times greater than that in the Decreased-P. Similarly, the inhomogeneity level of $Q$ is 1.6 times higher in the Increased-P than Decreased-P. This is because the events in the Increased-P group have a higher background air temperature (i.e. over the urban area) than the events in the Decreased-P group. The urban sensible heat flux in the Increased-P group is acting to enhance the UHI, resulting in a higher spatial variability of $T$ between the urban area and its surroundings as well. Moreover, the Increased-P events show a greater urban-surrounding difference in $Q$ values. The decreased evapotranspiration resulting from the prevalence of impervious urban land (Huang *et al* 2022), coupled with enhanced surface atmosphere heating, leads to the UDI effect that is expressed by lower $Q$ values over the urban area. In summary, it appears that convective rainfall events classified as Increased-P are characterized by strong UHI and UDI effects that result in a high thermodynamic inhomogeneity (i.e. a large contrast between the urban area and its surroundings, further details can be found in cross-section analysis in figure S8).

Last, we investigate the timing of the rainfall and heat anomalies caused by further urban expansion in the future, focusing on the difference between the present urban area (CTR) and future urban growth (Urban-2 km). We found that 82% of the rainfall in the Increased-P group occurs during the day, whereas 65% of the rainfall in the Decreased-P group occurs at night (figure 3). The diurnal pattern of $\delta P_{u2}$ and $\Delta T_{u2}$ seems to agree; thus, we examine this relationship in more detail. Urban growth leads to a consistent rise in the daytime temperature within the urban area, as evident by $\Delta T_{u2}$ being positive from 08:00 to 23:00 LST and negative between 23:00 and

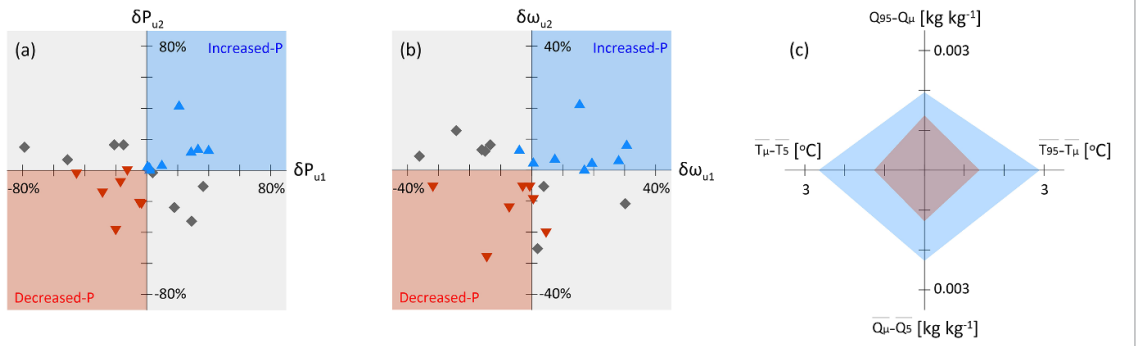


**Figure 2.** (a) A scatter plot of the differences in urban rainfall for the 23 simulated storms between No-urban and CTR ($\delta P_{u1}$) and CTR and Urban-2 km ($\delta P_{u2}$) scenarios. (b) Similar scatter plot as in (a) but for $\omega$. (c) A radar plot of the 5–95th percentile differences from the mean temperature $T$ and water vapor mixing ratio $Q$ in the Increased-P (blue area) and Decreased-P (red area) groups in the CTR scenario. The detailed information in panel (c)—All pooled values of $\hat{T}_i^u(t)$ and $\hat{T}_i^s(t)$, and of $\hat{Q}_i^u(t)$ and $\hat{Q}_i^s(t)$, for the CTR scenario are shown in the box plots in figure S6; the non-pooled data for all scenarios are presented as box plots in figure S7.

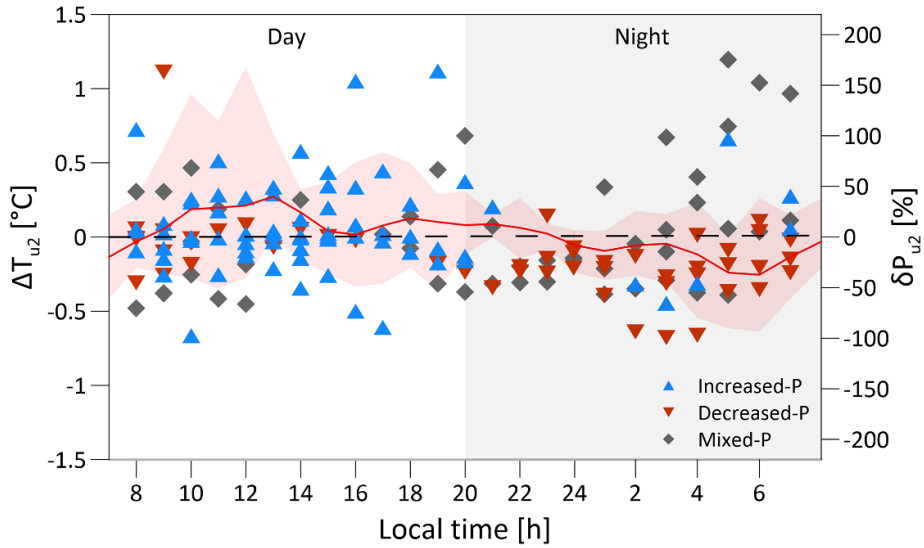


**Figure 3.** The diurnal pattern of urban-surrounding temperature difference ($\Delta T_{u2}$) and relative rainfall anomalies ($\delta P_{u2}$) from CTR to Urban-2 km scenarios. The red line represents the average hourly $\Delta T_{u2}$ obtained from all simulated events (the colored area is the 5–95th percentile range). The dots represent hourly $\delta P_{u2}$ of simulated events, divided into the Increased-P, Decreased-P, and Mixed-P groups. Daytime in Shanghai is from 8:00 to 20:00 LST.

07:00 LST. The likelihood of $\delta P_{u2}$ being positive is also higher during the daytime, particularly in the afternoon (13:00–18:00 LST), and reaches its greatest increase at 15:00 LST. Conversely, during the night, the probability of $\delta P_{u2}$ being negative increases, peaking at midnight. This implies that extended urbanization positively impacts rainfall from noon through late afternoon but has a negative impact at night. Yet we note that urban relative humidity tends to increase in the early morning (03:00–07:00 LST; figure S9). This is because the city's temperature is not as high as it is during the day, which leads to less dew accumulation compared to the surrounding area, causing excess moisture that forms a distinct 'moisture island' within the city (see also Chow and Chang 1984). This additional moisture tends to favor intense rainfall over the city, as indicated by some data points above the zero-line from 03:00 to 07:00 LST in figure 3 and also an increasing percentage of positive $\delta P_{u2}$ in figure S10.

## 4. Urban thermodynamic processes

Based on the results of our numerical experiment, we attempt to interpret the mechanisms controlling urban expansion's impact on short-duration convective rainfall in Shanghai. A schematic representation of these thermodynamic mechanisms is provided in figure 4, which summarizes our interpretation of urbanization-induced rainfall processes for a subtropical city. Daytime rainfall (especially in the afternoon from 13:00 to 18:00 LST) is impacted by urban temperature increases (UHI effect) and water vapor mixing ratio depressions (UDI effect), which cause

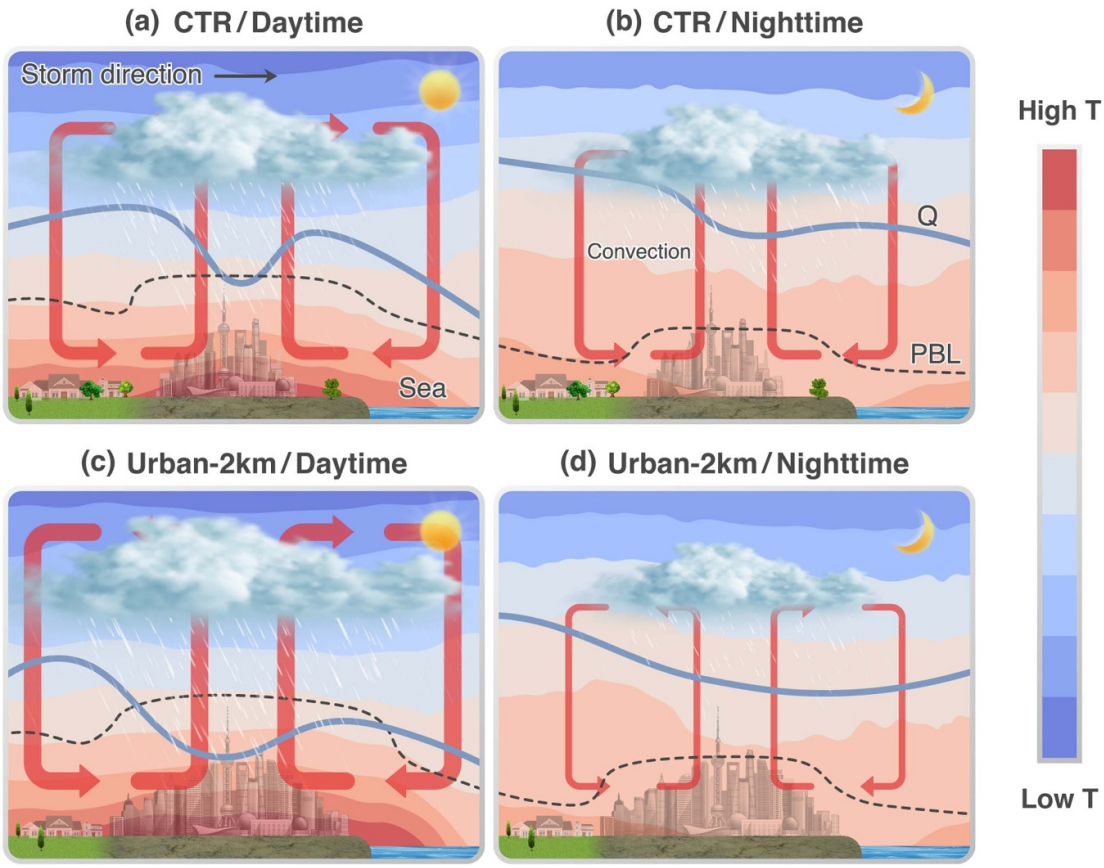


**Figure 4.** A schematic illustration of urbanization effect on short-duration convective rainfall in a subtropical city. 'CTR' in (a) and (b) refers to the reference city, while 'Urban-2 km' in (c) and (d) refers to the urban expansion of the reference city by 2 km. Values of $T$ (air temperature, from 2 m up to a height of 1.5 km), $Q$ (water vapor mixing ratio at 2 m), and PBL (planetary boundary layer height) are conceptualized based on the analysis of 23 rainfall events presented in section 2.1. The cross-section coordinates are in figure S8(e).

thermodynamic disturbances in air pressure, intensifying vertical movements at the edge of the urban area, and making the atmosphere more unstable (figure 4(a)). At night, the land-atmospheric coupling is usually weaker compared to during the day, hence, the urban influence on rainfall is less pronounced. Consequently, the temperature and moisture are observed to be uniformly distributed among the city and its surroundings (figure 4(b)), resulting in less convection development and rainfall.

With urban expansion (Urban-2 km simulations), UHI and UDI intensify throughout daytime, and as a result, urban areas experience even higher temperatures than the surrounding area and larger humidity depression (figure 4(c)). This leads to an elevated planetary boundary layer (PBL) (see also Wang *et al* 2015, Hu *et al* 2022) that increases the horizontal moisture convergence (Zhang *et al* 2019). Coupled with stronger thermally induced circulations (in agreement with Zhang *et al* 2014), this enhances cloud development and increases rainfall amounts.

On the contrary, the city expansion leads to even more homogeneous temperature and moisture distribution at night (in comparison with the reference city), thereby increasing the atmospheric stability (figure 4(d)). The urbanization-induced surface moisture depression and consequently vertical motion decrease are the primary reasons for rainfall reduction during the night, which is consistent with the findings of Zhang *et al* (2009).

## 5. Discussion

In a few events, changes in $\overline{\hat{P}_i^u}$ with urbanization did not follow $\overline{\hat{\omega}_i^u}$ in (figure 2). For example, Event 1 (table S1) in the Increased-P group has a 'mixed' $\overline{\hat{\omega}_i^u}$. This event is the longest we simulate (i.e. 15 h), and the urbanization scenarios triggered an earlier onset and a later cessation of the urban rainfall, thus affecting the statistical analysis. Rainfall starts earlier because of the increased sensible heat flux, which triggers the development of convective clouds in the urbanized area (Zhang *et al* 2017). Furthermore, increased urban roughness may slow down the propagation of the storms, prolong rainfall duration, and further facilitate the enhancement of rainfall in urban areas (Bornstein and Lin 2000, Thielen *et al* 2000, Wan and Zhong 2014, Yu and Liu 2015). Events 5 and 9

in the Decreased-P group (table S1) are also associated with a 'mixed' $\overline{\hat{\omega}_i^u}$ but occur at night (23:00 LST), a time which is associated with a weak UHI effect (see figure S8). For these events, decreased rainfall is mainly attributed to depression in relative humidity.

Although we only discuss the urbanization effect on the intensification of rainfall amounts here, some events also exhibit greater spatial variability as urban expansion increases (not shown here), which is consistent with our previous studies in Shanghai (Zhuang *et al* 2022) and also in Mumbai, India, as reported by Paul *et al* (2018). It sheds light on how urbanization influences rainfall spatial patterns.

Urbanization and urban expansion impacts on rainfall can be more diversified in coastal cities or cities close to water bodies with an abundance of moisture supply from the environment (Shepherd *et al* 2010, Theeuwes *et al* 2013, Yang *et al* 2014, Xing *et al* 2019). Also in our case study, localized water vapor depression is observed in the low-level atmosphere (see cross-section in figures S8(c) and (d)), while overall higher water vapor is evident in the entire Shanghai domain (see box plots comparing mean values between $\hat{Q}_i^u(t)$ and $\hat{Q}_i^s(t)$ in figures S7(c) and (d)). This is because urbanization leads to enhanced lower-level convergence, promoting the transportation of water vapor from the surroundings to urban areas. Besides, Shanghai, because of its location between the East China Sea and Taihu Lake, facilitates the convergence of water vapor from both the west and east sides of the city, resulting in increased $Q$ across the city's boundary. This mechanism also triggers enhanced vertical movement of water vapor, enhancing the atmospheric circulation between the urban and surrounding areas, and intensifying rainfall as a result. Therefore, coastal or lakeside urban settings would mitigate urbanization-induced moisture deficit effect in the lower atmosphere to a certain extent, by enhancing moist convection, which was also found in Xiong'an, China (Xing *et al* 2019), Milwaukee, United States (Yang *et al* 2014), and Tokyo, Japan (Inoue and Kimura 2004).

Sea breezes are expected to play a significant role in coastal urban areas. Overall, however, the contribution of sea-breeze is not clear in our cases, as we have limited samples (i.e. 5 storms) with sea-breeze occurring and the changes in the sea breeze strength are not considerably different between the Increased-P and Decreased-P groups. Several studies emphasized that urban-induced rainfall anomalies could differ in coastal and inland cities in the same climate region due to interactions between urban-rural circulation and sea breeze (Zhang *et al* 2022, Lalonde *et al* 2023, Lu *et al* 2024). Hence, we would suggest treating the transferability of our findings between cities with care. Our findings will likely be valid in other subtropical coastal cities that share similar climate characteristics with Shanghai, such as cities in the Southeast Coast of China (Jia *et al* 2023), Miami and Houston in the United States (Buran and Shepherd 2005, Misra *et al* 2018), among others.

Moreover, we have not examined the potential impacts of changes in aerosol amounts and composition following urbanization on rainfall, as we only focus on the thermal-dynamic effects. Future studies should include a comprehensive analysis of the consideration of aerosols (Persad 2023) and anthropogenic heat emissions (Marelle *et al* 2020) impact on urban rainfall.

## 6. Conclusions

We utilized a convection-permitting model to examine the potential effects of urbanization on heavy short-duration summer convective storms in Shanghai, China. The simulation of 23 storms with varying durations and timing under three urban setup scenarios indicated that an increase in urban extent does not necessarily lead to an increase in storm intensity. Our results highlight the importance of urban-surrounding hydrothermal differences, especially during the day when land-atmosphere coupling is strong. Urban expansion amplifies temperature and moisture differences between the city and its surrounding areas during daytime, enhancing the convection and rainfall. Conversely, with more uniform temperature and moisture distribution at night, urbanization suppresses convection initiation and consequently rainfall intensity. These findings contribute to the understanding of the thermodynamic processes behind the contradictory response of convective rainfall to city expansion that can be expected in subtropical regions that share similar climate characteristics. While presenting a mixed response to urban expansion in terms of convective storms, we emphasize that as a result of growth in subtropical cities, an overall intensification of convective rainfall is likely, since most convective activity occurs during the day.

## Data availability statement

WRF model outputs ($\hat{P}_i(t)$, $\hat{T}_i(t)$, $\hat{Q}_i(t)$, and $\hat{\omega}_i(t)$) of the 23 simulated rainfall for the three urban scenarios over the domain presented in figure 1(c), are available at https://zenodo.org/records/10931297 (Zhuang and Koukoula 2024). Observations from rain gauges were obtained from the Shanghai Water Planning and Design Research Institute in China—access to these data, which were used under license, is subject to certain restrictions. The NCEP GFS 0.25 Degree Global Forecast dataset is available at https://doi.org/10.5065/D65D8PWK. The NCEP FNL (Final) Operational Global Analysis dataset is available at https://doi.org/10.5065/D6M043C6. The MODIS data can be downloaded at https://www2.mmm.ucar.edu/wrf/users/download/get_sources_wps_geog.html.

## Acknowledgments

Q Z acknowledges the support of the China Scholarship Council grant (CSC. Grant Number: 202206260164). M K and N P are supported by the Swiss National Science Foundation (SNSF), Grant 194649 ('Rainfall and floods in future cities'). S L and Z Z acknowledge the support from the National Natural Science Foundation of China (NSFC), Grants 42271031, 42371030, respectively.

## ORCID iDs

Qi Zhuang https://orcid.org/0000-0002-2964-8201
Marika Koukoula https://orcid.org/0000-0002-8437-7272
Shuguang Liu https://orcid.org/0000-0002-8637-4745
Zhengzheng Zhou https://orcid.org/0000-0002-4973-1619
Nadav Peleg https://orcid.org/0000-0001-6863-2934

## References

Bornstein R and Lin Q 2000 Urban heat islands and summertime convective thunderstorms in Atlanta: three case studies *Atmos. Environ.* **34** 507–16

Broxton P D, Zeng X, Sulla-Menashe D and Troch P A 2014 A global land cover climatology using MODIS data *J. Appl. Meteorol. Climatol.* **53** 1593–605

Burian S J and Shepherd J M 2005 Effect of urbanization on the diurnal rainfall pattern in Houston *Hydrol. Process.* **19** 1089–103

Changnon S A, Huff F A and Semonin R G 1971 METROMEX: an investigation of inadvertent weather modification *Bull. Am. Meteorol. Soc.* **52** 958–68

Chen F and Dudhia J 2001 Coupling an advanced land surface–hydrology model with the Penn State–NCAR MM5 modeling system. Part I: model implementation and sensitivity *Mon. Weather Rev.* **129** 569–85

Chen G, Li X, Liu X, Chen Y, Liang X, Leng J, Xu X, Liao W, Qiu Y and Wu Q 2020 Global projections of future urban land expansion under shared socioeconomic pathways *Nat. Commun.* **11** 537

Chow S D and Chang C 1984 Shanghai urban influences on humidity and precipitation distribution *GeoJournal* **8** 201–4

Doan Q, Chen F, Kusaka H, Dipankar A, khan A, Hamdi R, Roth M and Niyogi D 2022 Increased risk of extreme precipitation over an urban agglomeration with future global warming *Earth's Future* **10** e2021EF002563

Fischer E M, Sippel S and Knutti R 2021 Increasing probability of record-shattering climate extremes *Nat. Clim. Change* **11** 689–95

Freitag B M, Nair U S and Niyogi D 2018 Urban modification of convection and rainfall in complex terrain *Geophys. Res. Lett.* **45** 2507–15

Georgescu M, Broadbent A M, Wang M, Krayenhoff E S and Moustaoui M 2021 Precipitation response to climate change and urban development over the continental United States *Environ. Res. Lett.* **16** 044001

Georgescu M, Mahalov A and Moustaoui M 2012 Seasonal hydroclimatic impacts of Sun Corridor expansion *Environ. Res. Lett.* **7** 034026

Givati A and Rosenfeld D 2004 Quantifying precipitation suppression due to air pollution *J. Appl. Meteorol. Climatol.* **43** 1038–56

Gu H, Jin J, Wu Y, Ek M B and Subin Z M 2015 Calibration and validation of lake surface temperature simulations with the coupled WRF-lake model *Clim. Change* **129** 471–83

Guo X L, Fu D H and Wang J 2006 Mesoscale convective precipitation system modified by urbanization in Beijing city *Atmos. Res.* **82** 112–26

Han L, Wang L, Chen H, Xu Y, Sun F, Reed K, Deng X and Li W 2022 Impacts of long-term urbanization on summer rainfall climatology in Yangtze River Delta agglomeration of China *Geophys. Res. Lett.* **49** e2021GL097546

Hand L and Shepherd J 2009 An investigation of warm-season spatial rainfall variability in Oklahoma city: possible linkages to urbanization and prevailing wind *J. Appl. Meteorol. Climatol.* **48** 251–69

Hao L, Sun G, Huang X, Tang R, Jin K, Lai Y, Chen D, Zhang Y, Zhou D, Yang Z *et al* 2023 Urbanization alters atmospheric dryness through land evapotranspiration *npj Clim. Atmos. Sci.* **6** 149

He J, Chen D, Gu Y, Jia H, Zhong K and Kang Y 2022 Evaluation of planetary boundary layer schemes in WRF model for simulating sea-land breeze in Shanghai, China *Atmos. Res.* **278** 106337

Hong S-Y, Dudhia J and Chen S-H 2004 A revised approach to ice microphysical processes for the bulk parameterization of clouds and precipitation *Mon. Weather Rev.* **132** 103–20

Hu Y, Tan J, Grimmond S, Ao X, Yan Y and Liu D 2022 Observed and modeled urban heat island and sea-breeze circulation interactions: a Shanghai case study *J. Appl. Meteorol. Climatol.* **61** 239–59

Huang X, Jin K, Chen D, Zheng Q and Hao L 2022 Urbanization altered atmospheric humidity diurnally and seasonally through ecohydrological processes in five urban agglomerations in China *Environ. Res. Lett.* **17** 084032

Inoue T and Kimura F 2004 Urban effects on low-level clouds around the Tokyo metropolitan area on clear summer days *Geophys. Res. Lett.* **31** L05103

IPCC, Intergovernmental Panel on Climate Change 2023 *Climate Change 2021—The Physical Science Basis: Working Group I Contribution to the Sixth Assessment Report of the Intergovernmental Panel on Climate Change* (Cambridge University Press) (https://doi.org/10.1017/9781009157896.021)

Jia W, Ren G, Jin F, He J and Zhang P 2023 Spatial-temporal characteristics of the urban heat island effect in Xiamen, China *Urban Clim.* **52** 101725

Joseph B, Bhatt B C, Koh T Y and Chen S 2008 Sea breeze simulation over the Malay Peninsula in an intermonsoon period *J. Geophys. Res.* **113** D20122

Kain J S 2004 The Kain–Fritsch convective parameterization: an update *J. Appl. Meteorol.* **43** 170–81

Lalonde M, Oudin L and Bastin S 2023 Urban effects on precipitation: do the diversity of research strategies and urban characteristics preclude general conclusions? *Urban Clim.* **51** 101605

Li X, Koh T-Y, Entekhabi D, Roth M, Panda J and Norford L K 2013 A multi-resolution ensemble study of a tropical urban environment and its interactions with the background regional atmosphere *J. Geophys. Res. Atmos.* **118** 9804–18

Li X, Koh T, Panda J and Norford L K 2016 Impact of urbanization patterns on the local climate of a tropical city, Singapore: an ensemble study *J. Geophys. Res. Atmos.* **121** 4386–403

Li Y, Wang W, Chang M and Wang X 2021 Impacts of urbanization on extreme precipitation in the Guangdong-Hong Kong-Macau greater bay area *Urban Clim.* **38** 100904

Liang P and Ding Y 2017 The long-term variation of extreme heavy precipitation and its link to urbanization effects in Shanghai during 1916–2014 *Adv. Atmos. Sci.* **34** 321–34

Liu J and Niyogi D 2019 Meta-analysis of urbanization impact on rainfall modification *Sci. Rep.* **9** 7301

Li Y, Liu Y, Chen Y, Chen B, Zhang X, Wang W, Shu Z and Huo Z 2021b Characteristics of deep convective systems and initiation during warm seasons over China and its vicinity *Remote Sens.* **13** 4289

Liu Z, Zhan W, Bechtel B, Voogt J, Lai J, Chakraborty T, Wang Z, Li M, Huang F and Lee X 2022 Surface warming in global cities is substantially more rapid than in rural background areas *Commun. Earth Environ.* **3** 219

Lu Y, Yu Z, Albertson J D, Chen H, Hu L, Pendergrass A, Chen X and Li Q 2024 Understanding the influence of urban form on the spatial pattern of precipitation *Earth's Future* **12** e2023EF003846

Marelle L, Myhre G, Steensen B M, Hodnebrog Ø, Alterskjær K and Sillmann J 2020 Urbanization in megacities increases the frequency of extreme precipitation events far more than their intensity *Environ. Res. Lett.* **15** 124072

Martilli A, Clappier A and Rotach M W 2002 An urban surface exchange parameterisation for mesoscale models *Bound.-Layer Meteorol.* **104** 261–304

Meili N, Paschalis A, Manoli G and Fatichi S 2022 Diurnal and seasonal patterns of global urban dry islands *Environ. Res. Lett.* **17** 054044

Miao S, Chen F, Li Q and Fan S 2011 Impacts of urban processes and urbanization on summer precipitation: a case study of heavy rainfall in Beijing on 1 August 2006 *J. Appl. Meteorol. Climatol.* **50** 806–25

Misra V, Mishra A, Bhardwaj A, Viswanathan K, Schmutz D 2018 The potential role of land cover on secular changes of the hydroclimate of Peninsular Florida *npj Clim. Atmos. Sci.* **1** 5

Mlawer E J, Taubman S J, Brown P D, Iacono M J and Clough S A 1997 Radiative transfer for inhomogeneous atmospheres: RRTM, a validated correlated-k model for the longwave *J. Geophys. Res. Atmos.* **102** 16663–82

NCEP 2000 NCEP FNL operational model global tropospheric analyses, continuing from July 1999 (https://doi.org/10.5065/D6M043C6)

NCEP 2015 NCEP GFS 0.25 degree global forecast grids historical archive (https://doi.org/10.5065/D65D8PWK)

Niu G, Yang Z, Mitchell K E, Chen F, EK M B, Barlage M, Kumar A, Manning K, Niyogi D and Rosero E 2011 The community Noah land surface model with multiparameterization options (Noah-MP): 1. Model description and evaluation with local-scale measurements *J. Geophys. Res. Atmos.* **116** D12109

Niyogi D, Pyle P, Lei M, Arya S P, Kishtawal C M, Shepherd M, Chen F and Wolfe B 2011 Urban modification of thunderstorms: an observational storm climatology and model case study for the Indianapolis urban region *J. Appl. Meteorol. Climatol.* **50** 1129–44

Oke T R 1982 The energetic basis of the urban heat island *Q. J. R. Meteorol. Soc.* **108** 1–24

Paul S, Ghosh S, Mathew M, Devanand A, Karmakar S and Niyogi D 2018 Increased spatial variability and intensification of extreme monsoon rainfall due to urbanization *Sci. Rep.* **8** 3918

Persad G G 2023 The dependence of aerosols' global and local precipitation impacts on the emitting region *Atmos. Chem. Phys.* **23** 3435–52

Qian Y, Chakraborty T C, Li J, Li D, He C, Sarangi C, Chen F, Yang X and Leung L R 2022 Urbanization impact on regional climate and extreme weather: current understanding, uncertainties and future research directions *Adv. Atmos. Sci.* **39** 819–60

Rosenfeld D, Lohmann U, Raga G B, Dowd C D, Kulmala M, Fuzzi S, Reissell A and Andreae M O 2008 Flood or drought: how do aerosols affect precipitation? *Science* **321** 1309–13

Schmid P E and Niyogi D 2013 Impact of city size on precipitation-modifying potential *Geophys. Res. Lett.* **40** 5263–7

Shem W and Shepherd M 2009 On the impact of urbanization on summertime thunderstorms in Atlanta: two numerical model casestudies *Atmos. Res.* **92** 172–89

Shen L, Zhao C, Ma Z, Li Z, Li J and Wang K 2019 Observed decrease of summer sea-land breeze in Shanghai from 1994 to 2014 and its association with urbanization *Atmos. Res.* **227** 198–209

Shen Y and Yang L 2023 Divergent urban signatures in rainfall anomalies explained by pre-storm environment contrast *Geophys. Res. Lett.* **50** e2022GL101658

Shepherd J M and Burian S J 2003 Detection of urban-induced rainfall anomalies in a major coastal city *Earth Interact.* **7** 1–17

Shepherd J M, Carter M, Manyin M, Messen D and Burian S 2010 The impact of urbanization on current and future coastal precipitation: a case study for Houston *Environ. Plan.* B **37** 284–304

Skamarock W C, Klemp J B, Dudhia J, Gill D O, Liu Z, Berner J and Huang X Mesoscale and Microscale Meteorology Laboratory, National Center for Atmospheric Research 2019 A description of the advanced research WRF model version 4 *Technical Report, NCAR Technical Notes* NCAR/TN-556+STR (https://doi.org/10.5065/1DFH-6P97)

Statista Search Department 2024 Gross domestic product (GDP) of Shanghai municipality in China from 2013 to 2023 (available at: www.statista.com/statistics/802355/china-gdp-of-shanghai)

Tapper N J 1990 Urban influences on boundary layer temperature and humidity: results from Christchurch, New Zealand *Atmos. Environ.* B **24** 19–27

Theeuwes N, Solcerová A and Steeneveld G 2013 Modeling the influence of open water surfaces on the summertime temperature and thermal comfort in the city *J. Geophys. Res. Atmos.* **118** 8881–96

Thielen J, Wobrock W, Gadian A, Mestayer P G and Creutin J-D 2000 The possible influence of urban surfaces on rainfall development: a sensitivity study in 2D in the meso-gamma scale *Atmos. Res.* **54** 15–39

United Nations 2018 World urbanization prospects: the 2018 revision *Technical Report* (Department of Economic and Social Affairs, Population Division)

Van den Heever S C and Cotton W R 2007 Urban aerosol impacts on downwind convective storms *J. Appl. Meteorol. Climatol.* **46** 828–50

Wan H C and Zhong Z 2014 Ensemble simulations to investigate the impact of large-scale urbanization on precipitation in the lower reaches of Yangtze River Valley, China *Q. J. R. Meteorol. Soc.* **140** 258–66

Wang J, Feng J and Yan Z 2015 Potential sensitivity of warm season precipitation to urbanization extents: modeling study in Beijing Tianjin-Hebei urban agglomeration in China *J. Geophys. Res. Atmos.* **120** 9408–25

Wang J, Feng J and Yan Z 2018 Impact of extensive urbanization on summertime rainfallin the Beijing region and the role of local precipitation recycling *J. Geophys. Res. Atmos.* **123** 3323–40

Wang J, Feng J, Yan Z, Hu Y and Jia G 2012 Nested high-resolution modeling of the impact of urbanization on regional climate in three vast urban agglomerations in China *J. Geophys. Res.* **117** D21103

Xing Y, Ni G, Yang L, Yang Y, Xing P and Sun T 2019 Modeling the impacts of urbanization and open water surface on heavy convective rainfall: a case study over the emerging Xiong'an city, China *J. Geophys. Res. Atmos.* **124** 9078–98

Xu P, Wang D, Wang Y, Wu J, Heng Y, Singh V P, Liu C, Wang L, Shang X and Fang H 2024 Quantifying the urbanization and climate change-induced impact on changing patterns of rainfall intensity-duration-frequency via nonstationary models *Urban Clim.* **55** 101990

Yang L, Smith J A, Baeck M L, Bou-Zeid E, Jessup S M, Tian F and Hu H 2014 Impact of urbanization on heavy convective precipitation under strong large-scale forcing: a case study

over the Milwaukee–Lake Michigan region *J. Hydrometeorol.* **15** 261–78
Yang L, Smith J and Niyogi D 2019 Urban impacts on extreme monsoon rainfall and flooding in complex terrain *Geophys. Res. Lett.* **46** 5918–27
Yang P, Ren G and Yan P 2017 Evidence for a strong association of short-duration intense rainfall with urbanization in the Beijing urban area *J. Clim.* **30** 5851–70
Yu M and Liu Y 2015 The possible impact of urbanization on a heavy rainfall event in Beijing *J. Geophys. Res. Atmos.* **120** 8132–43
Zhang C, Chen F, Mao S, Li Q, Xia X and Xuan C 2009 Impacts of urban expansion and future green planting on summer precipitation in the Beijing metropolitan area *J. Geophys. Res. Atmos.* **114** 0148–227
Zhang H, Wu C, Chen W and Huang G 2019 Effect of urban expansion on summer rainfall in the Pearl River Delta, South China *J. Hydrol.* **568** 747–57
Zhang N, Wang X and Peng Z 2014 Large-eddy simulation of mesoscale circulations forced by inhomogeneous urban heat island *Bound.-Layer Meteorol.* **151** 179–94
Zhang W, Villarini G, Vecchi G A and Smith J A 2018 Urbanization exacerbated the rainfall and flooding caused by hurricane Harvey in Houston *Nature* **563** 384–8
Zhang W, Yang J, Yang L and Niyogi D 2022 Impacts of city shape on rainfall in inland and coastal environments *Earth's Future* **10** e2022EF002654
Zhang Y, Miao S, Dai Y and Bornstein R 2017 Numerical simulation of urban land surface effects on summer convective rainfall under different UHI intensity in Beijing *J. Geophys. Res. Atmos.* **122** 7851–68
Zhao J, Yang L, Li L, Wang L, Hu Q and Wang Y 2020 Analysis of the lake-effect on precipitation in the Taihu lake basin based on the GWR merged precipitation *Water* **12** 180
Zhao L, Lee X, Smith R B and Oleson K 2014 Strong contributions of local background climate to urban heat islands *Nature* **511** 216–9
Zhong S, Qian Y, Zhao C, Leung R, Wang H, Yang B, Fan J, Yan H, Yang X and Liu D 2017 Urbanization-induced urban heat island and aerosol effects on climate extremes in the Yangtze River Delta region of China *Atmos. Chem. Phys.* **17** 5439–57
Zhu X, Gao W, Zhou N, Kammen D M, Wu Y, Zhang Y and Chen W 2016 The inhabited environment, infrastructure development and advanced urbanization in China's Yangtze River Delta region *Environ. Res. Lett.* **11** 124020
Zhu Y and Ling G H T 2024 Spatio-temporal changes and driving forces analysis of urban open spaces in Shanghai between 1980 and 2020: an integrated geospatial approach *Remote Sens.* **16** 1184
Zhuang Q and Koukoula M 2024 Urbanization numerical experiment in Shanghai: WRF model outpts (Zenodo) (https://doi.org/10.5281/zenodo.10931297)
Zhuang Q, Zhou Z, Liu S, Wright D B, Tavares Araruna Júnior J, Makhinov A N and Makhinova A F 2022 Bivariate rainfall frequency analysis in an urban watershed: combining copula theory with stochastic storm transposition *J. Hydrol.* **615** 128648